Coordinated Derived Current Control of DFIG's RSC and GSC Without PLL Under Unbalanced Grid Voltage Conditions

Cheng, Peng; Wu, Chao; Ma, Jing; Blaabjerg, Frede

Published in:
IEEE Access

DOI (link to publication from Publisher):
10.1109/ACCESS.2020.2984541

Publication date:
2020

Document Version
Publisher's PDF, also known as Version of record

IEEE Access
Multidisciplinary | Rapid Review | Open Access Journal

Received March 9, 2020, accepted March 26, 2020, date of publication March 31, 2020, date of current version April 16, 2020.

Digital Object Identifier 10.1109/ACCESS.2020.2984541

Coordinated Derived Current Control of DFIG's RSC and GSC Without PLL Under Unbalanced Grid Voltage Conditions

PENG CHENG[1], CHAO WU[2], (Member, IEEE), JING MA[1], (Senior Member, IEEE), AND FREDE BLAABJERG[2], (Fellow, IEEE)

[1]China Institute of Energy and Transportation Integrated Development, North China Electric Power University, Beijing 102206, China
[2]Department of Energy Technology, Aalborg University, 9220 Aalborg, Denmark

Corresponding author: Chao Wu (cwu@et.aau.dk)

This work was supported in part by the National Natural Science Foundation of China under Grant 51807182, in part by the National Key Research and Development Program of China under Grant 2018YFB0904003, and in part by the Science and Technology Project of State Grid Corporation of China under Grant NYB17201900282.

ABSTRACT This paper proposes a coordinated derived current control strategy of doubly fed induction generator (DFIG) system under unbalanced grid voltage conditions. The rotor-side converter (RSC) and the grid-side converter (GSC) are synchronized to the grid with a virtual phase angle of nominal frequency, which can be simply set as $\theta = \omega_n t$ ($\omega_n = 100\pi$). Consequently, the proposed control strategy can implement in an arbitrary reference frame without phase-locked loop (PLL). The derived d-q axis currents are obtained from the DFIG stator and GSC currents with virtual angle-based Park Transformations. For a simple implementation, a reduced-order vector integrator with a voltage vector multiplier is used to directly regulate the measured powers/currents containing both the dc part and the oscillating part without sequence extractions. By this means, RSC achieves torque ripple reduction and then GSC can rebalance the currents and smooth the active/reactive powers. Finally, the experimental results on a small laboratory setup are presented to validate the effectiveness of the proposed control strategy.

INDEX TERMS Doubly fed induction generator, derived current control, coordinated control, unbalanced voltage.

NOMENCLATURE

$\boldsymbol{U}_s, \boldsymbol{I}_s$	Stator voltage and current vectors.
$\boldsymbol{U}_r, \boldsymbol{I}_r$	Rotor voltage and current vectors.
$\boldsymbol{U}_g, \boldsymbol{I}_g$	Grid-side voltage and current vectors
$\boldsymbol{\psi}_s, \boldsymbol{\psi}_r$	Stator, rotor flux linage vectors.
R_s, R_r	Stator, rotor resistances.
L_m	Mutual inductances.
L_s, L_r	Stator, rotor self-inductances.
$L_{\delta s}, L_{\delta r}$	Stator, rotor leakage inductances.
L_g, R_g	Input inductance and resistance of GSC.
$\omega_n, \omega_g, \omega_r$	Nominal grid, actual grid and rotor angular frequencies.
$\theta_{RSC}, \theta_{GSC}$	Virtual phase angles of RSC and GSC.
P_s, Q_s	Stator output active and reactive powers.
P_g, Q_g	Grid-side output active and reactive powers.
P_t, Q_t	Total output active and reactive powers of DFIG system.

The associate editor coordinating the review of this manuscript and approving it for publication was Firuz Zare.

I. INTRODUCTION

In decades, the transport electrification, especially the electrified train and the electric vehicles, has attracted more extensive attention due to lower carbon emissions and higher energy-efficiency than the fossil fuel-powered trains and vehicles. The International Renewable Energy Agency forecasts that the share of renewable electricity in the transport sector rises from just 0.3% in 2016 to 37% in 2050 [1]. Therefore, the integration of more renewable energy in the transport sector is the key factor for locally producing clean energy to supply the increasing electricity demand.

Wind power generation, as the promising renewable energy generation, will gain the increasing growth with the prediction of installed capacity over 6000 GW in 2050, which is dominated by doubly fed induction generators (DFIGs) [1], [2]. However, as the numbers of electrified trains and electric vehicles, the heavy and unbalanced loads due to traction power and charging power may cause the voltage unbalance for local grid [3], [4]. This would cause unbalanced currents and pulsating power/ torque and even lead to the

disconnection of the DFIGs, which is not allowed by issued grid codes [5], [6].

Focused on the slight long-time voltage unbalance, the currents behave as dc signals and ac signals as twice the grid frequency in the synchronous reference frame. The multiple-frequency current controllers, such as dual PI controller [7] and PI-R controller [8] are employed to regulate the dual-sequence current. In [9], four available targets for DFIGs are defined based on the positive- and negative-sequence voltages and currents with generator parameters. However, they are difficult for accurate extraction of the positive- and negative-sequence voltages and currents. Meanwhile, the generator parameters may always change with variable conditions. In [10], [11], the direct resonant control is developed, where the resonant controllers are employed to directly regulate the oscillating signal without extraction of dual-sequence currents and voltages. The strategies in [7]–[11] are implemented in the synchronous reference frame, which is oriented with the grid voltage by phase-locked loop (PLL). As indicated in [12], [13], the PLL would introduce a negative resistor with a negative impact on the converter stability. Several design methods of PLL, e.g., the impedance-based method [14] and the symmetrical optimum method [15], have been studied. However, the designed PLL parameters are closely related to the grid impedance and the design process is relatively complicated with more additional efforts. Thus, for a simple implementation, the control strategy without PLL is needed.

Direct power control (DPC) serves as a PLL-less method and has been widely studied. In [16], [17], a grid voltage modulated-DPC is proposed with the feed-forward and feedback controllers. In [18], a virtual phase angle is used for coordinate transformations in the place of the voltage phase angle from PLL and then based on this, an improved DPC is developed. Due to the absence of the PLL, the negative impacts of the PLL can be avoided. However, in practice, the grid-connected currents are preferred to be controlled as a general requirement. For this issue, the vector current control without PLL is derived from DPC [19]. It synchronizes with the grid voltage through the power calculation instead of the PLL. However, the synchronization would be deteriorated due to the power pulsations caused by unbalanced voltages. In [20], [21], the stator current control of DFIGs is developed in the arbitrary reference frame. It can improve the generator performance under unbalanced grid voltage conditions. However, the overall grid-connected performance of DFIG system is determined not only by the generator but also by the GSC, which can serve as a compensator for enhanced operation, e.g., balanced currents, smooth active power and smooth reactive power. Thus, for unbalanced issues, the coordinated control of RSC and GSC is preferred.

This paper presents a coordinated derived current control of RSC and GSC without PLL under unbalanced grid voltage conditions. In the control strategy, the controlled d-q axis currents are derived from the stator and converter currents through a virtual phase angle without PLL. But the active and reactive currents are coupled in the derived d- and q axis currents due to PLL's absence. For the predefined modes of the overall DFIG system, a reduced-order vector integrator (ROVI) multiplied by the voltage vector is designed to regulate the pulsating components without sequence extraction. By this means, RSC achieves torque ripple reduction and then GSC can rebalance total currents and smooth total active/reactive powers, which is helpful for the integration of DFIG-based wind power generation in the transport sector. If the network is harmonic/inter-harmonic, similar controllers will be designed on this basic control scheme in the future work. In Section II, the mathematic model is presented. Then, Section III gives the control system. In Section IV, the experimental validation is conducted. Finally, Section V summarizes the results in conclusion.

II. MATHEMATIC MODEL

A generalized vector $\boldsymbol{F}$ is used to represent voltage $\boldsymbol{U}$, current $\boldsymbol{I}$ or flux linkage $\boldsymbol{\psi}$. Since positive and negative-sequence signals are of the same frequency in the stationary reference frame, the generalized vector is expressed as

$$\boldsymbol{F} = F_+ \cdot e^{j\omega_g t} + F_- \cdot e^{-j\omega_g t} \tag{1}$$

where ω_g is the actual angular frequency, subscripts $+$, $-$ refers to the positive and negative sequence components.

Then, an arbitrary phase angle is produced by the nominal angular frequency $\omega_{\rm n} = 100\pi$ rad/s. Based on this phase angle, Park Transformations are carried out and the generalized vector $\boldsymbol{F}$ in the virtual phase angle-oriented (dq) reference frame is expressed as,

$$\boldsymbol{F}_{dq} = F_+ \cdot e^{j(\omega_g - \omega_{\rm n})t} + F_- \cdot e^{-j(\omega_g + \omega_{\rm n})t} \tag{2}$$

The virtual phase angle-oriented (dq) reference frame will always rotate at $\omega_{\rm n} = 100\pi$ rad/s regardless of the actual grid angular frequency. Thus, in the virtual phase angle-oriented (dq) reference frame, the derived positive sequence components are of $|\omega_g - \omega_{\rm n}|$, while the derived negative sequence components are of $|\omega_g + \omega_{\rm n}|$. It is noted that the frequency of dual-sequence components is not fixed but will vary in a narrow range due to frequency deviations.

A. RSC(DFIG)

Figure 1 gives DFIG's equivalent circuit in the virtual phase angle-oriented (dq) reference frame. In RSC, a virtual phase angle $\theta_{\rm RSC} = \omega_{\rm n} t$ is employed for coordinate transformations. Accordingly, the expressions of voltage and flux linkage can be obtained as,

$$\begin{cases} \boldsymbol{U}_{sdq} = R_s \boldsymbol{I}_{sdq} + d\boldsymbol{\psi}_{sdq}/dt + j\omega_n \boldsymbol{\psi}_{sdq} \\ \boldsymbol{U}_{rdq} = R_r \boldsymbol{I}_{rdq} + d\boldsymbol{\psi}_{rdq}/dt + j(\omega_n - \omega_{\rm r})\boldsymbol{\psi}_{rdq} \end{cases} \tag{3}$$

$$\begin{cases} \boldsymbol{\psi}_{sdq} = L_s \boldsymbol{I}_{sdq} + L_m \boldsymbol{I}_{rdq} \\ \boldsymbol{\psi}_{rdq} = L_m \boldsymbol{I}_{sdq} + L_r \boldsymbol{I}_{rdq} \end{cases} \tag{4}$$

where $R_{\rm s}$ and $R_{\rm r}$ are stator and rotor resistances, $\omega_{\rm r}$ is rotor angular frequency, $L_{\rm m}$ is mutual inductance, $L_{\delta s}$ and $L_{\delta r}$ are stator and rotor leakage inductances, $L_s = L_m + L_{\delta s}$ and $L_r = L_m + L_{\delta r}$ are stator and rotor self-inductances, respectively.

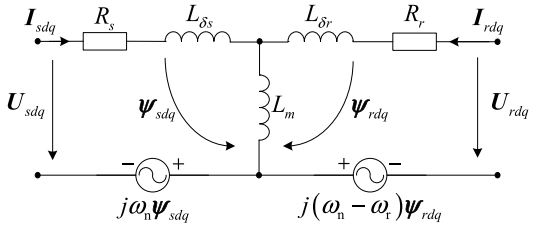

FIGURE 1. Equivalent circuit.

Then, the rotor flux linkage is expressed in the terms of the stator flux linkage and current as,

$$\boldsymbol{\psi}_{rdq} = L_s\boldsymbol{\psi}_{sdq}/L_m - L_{\delta sr}\boldsymbol{I}_{sdq} \tag{5}$$

where $L_{\delta sr} = L_s \cdot L_r/L_m - L_{\mathrm{m}}$.

Based on (3) and (5), the rotor voltage is represented as,

$$\boldsymbol{U}_{rdq} = \boldsymbol{E}_{rdq} - (L_rR_s + L_sR_r)/L_m\boldsymbol{I}_{sdq} - L_{\delta sr}d\boldsymbol{I}_{sdq}/dt \tag{6}$$

where $\boldsymbol{E}_{rdq}$ is decoupling voltage and given as,

$$\begin{aligned}\boldsymbol{E}_{rdq} = {} & \frac{L_r}{L_m}\left[\boldsymbol{U}_{sdq} + (R_r/L_r - j\omega_r)\,\boldsymbol{\psi}_{sdq}\right] \\ & -j(\omega_n - \omega_r)L_{\delta sr}\boldsymbol{I}_{sdq}\end{aligned} \tag{7}$$

For a practical DFIG, since the rotor self-inductance L_r is much larger than the rotor resistance R_r, the term R_r/L_r can be nearly regarded as zero. Accordingly, the expression (7) can be simplified as,

$$\boldsymbol{E}_{rdq} = L_r\left[\boldsymbol{U}_{sdq} + j\omega_r\boldsymbol{\psi}_{sdq}\right]/L_m - j(\omega_n - \omega_r)L_{\delta sr}\boldsymbol{I}_{sdq} \tag{8}$$

As seen from (6) and (8), the rotor voltage is calculated in the terms of the stator current and the decoupling voltage in d-q axis model without the PLL. The derived d-q axes stator currents are set as controlled variables instead of the rotor currents in conventional vector control or the stator powers in DPC. It refers to a novel derived current control approach of the grid-connected DFIG in the virtual phase angle-oriented (dq) reference frame. Noted that, since the virtual phase angle-oriented (dq) reference frame is not along with the stator voltage, there are both active and reactive components in the d- or q-axis current. Besides, the derived currents will vary in a narrow range due to the allowed frequency deviation.

B. GSC

In GSC, another virtual phase is set as $\theta_{\mathrm{GSC}} = \omega_{\mathrm{n}}t$ at nominal frequency for coordinate transformations. Noted that, although θ_{GSC} for GSC and θ_{RSC} for RSC are of the same expression, the calculation starts at different moments due to GSC and RSC implemented by two independent converters. Thus, the virtual phase angle of GSC is unrelated to that of RSC. It means that the information exchange on the virtual phase angle between two converters are not needed. Then, the derived currents of GSC in the virtual phase angle-oriented (dq) reference frame are obtained as,

$$\boldsymbol{I}_{gdq} = \boldsymbol{I}_{gdq+} \cdot e^{j(\omega_g - \omega_n)t} + \boldsymbol{I}_{gdq-} \cdot e^{-j(\omega_g + \omega_n)t} \tag{9}$$

For the GSC, the dynamic equations consisting of the output voltages, the grid voltages and the derived currents in the virtual phase angle-oriented (dq) reference frame can be expressed as,

$$\boldsymbol{V}_{cdq} = \boldsymbol{E}_{cdq} - R_g\boldsymbol{I}_{gdq} - L_g\frac{d}{dt}\boldsymbol{I}_{gdq} \tag{10}$$

where $\boldsymbol{V}_{cdq}$ is the output voltage, $\boldsymbol{U}_{gdq}$ is the grid voltage, $\boldsymbol{E}_{cdq}$ is the decoupling voltage term, respectively.

$$\boldsymbol{E}_{cdq} = \boldsymbol{U}_{gdq} - j\omega_{\mathrm{n}}L_g\boldsymbol{I}_{gdq} \tag{11}$$

As seen, the control inputs in (10) are represented in d-q model without PLL. The derived currents from the output currents can be set as new controllable variables.

However, since the virtual phase angle-oriented (dq) reference frame is not coincident with the voltage vector, the active and reactive powers are coupling the derived d-q axis currents. There are no proportional relationship of the d-axis current and the active power and the q-axis current and the reactive power in the d-axis voltage oriented reference frame. Due to allowed frequency deviations, the nominal frequency mismatches the actual frequency. The frequency of dual-sequence components in virtual phase angle-oriented reference frame is not fixed but varies in a narrow range. In other words, the frequency of the positive sequence signals is in low-frequency bandwidth, while that of the negative sequence signals are around twice the grid frequency. Thus, the coupling between the active-reactive powers and the d-q axis currents and the frequency mismatch must be considered for the control system.

III. CONTROL SYSTEM

A. CONTROLLER DESIGN

In the virtual phase angle-oriented (dq) reference frame, since the derived current is of dual frequencies, two controllers are needed. One is to regulate the positive sequence current for power tracking. The other one is for the negative sequence current to achieve enhanced performance.

Under ideal grid ($\omega_g = \omega_{\mathrm{n}}$), positive sequence currents are dc signals in the virtual phase angle-oriented reference frame, while the negative sequence currents are twice the grid frequency signals. Thus, a PI and ROVI tuned at twice the grid frequency are used and the expressions are given as,

$$\mathrm{G_{PI}}(s) = k_{\mathrm{p}} + \frac{k_i}{s} \tag{12}$$

$$G_{\mathrm{ROVI}}(s) = \frac{k_{\mathrm{r1}} + k_{\mathrm{r2}}s}{s + j2\omega_n} \tag{13}$$

where k_{p} and k_{i} are the proportional and integral parameters, k_{r1} and k_{r2} are the first and second resonant parameters.

In practice, the actual frequency ω_g is usually around the nominal one ω_{n}, but not always equal to the nominal one ω_{n}. Under such cases, the positive sequence components are not dc signals, but at $|\omega_g - \omega_{\mathrm{n}}|$, while the negative sequence components are at $|\omega_g + \omega_{\mathrm{n}}|$ around twice the grid frequency. It is noted that the allowed frequency deviation in grid codes is

in a relatively narrow range of ±0.5Hz and ±1.0Hz [22], [23]. As a result, the frequency of the positive sequence signals are under 1.0 Hz in the virtual phase angle-oriented (dq) reference frame, which can be nearly regarded as quasi dc signals. The PI controller is still able to regulate the quasi dc signals due to sufficient amplitude gain in such bandwidth.

Against frequency sensitivity, a cut-off angular frequency $\omega_c = 5\sim30$ rad/s is introduced in order to reduce its sensitivity at the resonant frequency. Then, (13) can be re-written as,

$$G_{ROVI}(s) = \frac{\omega_c\,(k_{r1} + k_{r2}s)}{s + j2\omega_n + \omega_c} \tag{14}$$

Based on (6) and (10), the relationship between k_{r1} and k_{r2} are calculated with pole-zero cancellation, as $k_{r1} = R_g/L_g \cdot k_{r2}$ for GSC and $k_{r1} = (L_r R_s + L_s R_r)/(L_s L_r - L2\,m)\cdot k_{r2}$ for RSC.

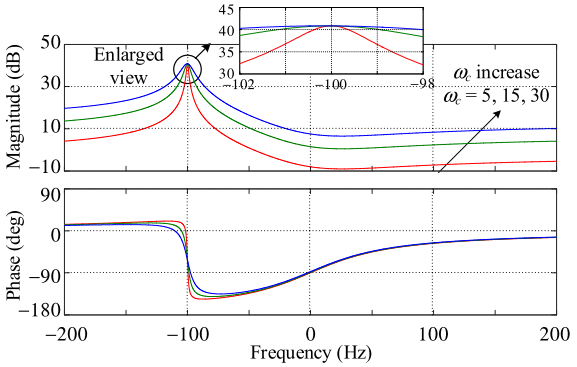

FIGURE 2. Bode diagram of ROVIs for RSC (k_{r1} =100, $k_{r2} = k_{r1}/320$=0.312).

Figure 2 gives ROVI's bode diagrams for RSC with ω_c = 5, 15, 30 rad/s based on the parameters in Table 1. The positive and negative frequency refers to the positive and negative rotating direction of ac signals. It is seen that the amplitude values of the ROVIs at the resonant frequency are larger than 40 dB regardless of different cut-off frequencies, which is enough to regulate the twice grid frequency signals. Besides, the ROVI can afford the separation of the positive and negative sequence signals due to the single-side resonance, which can prevent the 3rd-order harmonic signals generating.

TABLE 1. Parameters of laboratory setup.

Rated power	1.0 kW	Rated voltage	110 V
Rated frequency	50 Hz	R_s	1.01 Ω
Turns ratio	0.33	dc-link voltage	200 V
R_r	0.88 Ω	L_m	90.1 mH
$L_{\delta s}$	3.0 mH	$L_{\delta r}$	3.0 mH
R_g	0.2 Ω	L_g	2.5 mH
V_{dc}	200V	C_{dc}	780 μF

Considering the allowed frequency deviation in [22], [23], the frequency of the negative sequence currents varies between 99.0 Hz and 101.0 Hz in the virtual phase angle-oriented (dq) reference frame. Besides, the frequency of the oscillating power/torque are at $2\omega_g$ between 98.0 Hz and 102.0 Hz. In the enlarged view in Figure 2, the minimum magnitude values in the bandwidth 98.0∼102.0 Hz are decreased to 33.8 dB, 38.5 dB and 40.1 dB when ω_c = 5, 15, 30 rad/s, respectively. However, these magnitude gains are large enough to control the ac signals around twice the grid frequency caused by unbalanced voltages. Thus, the ROVI can still satisfactorily work if there are frequency deviations.

B. MODULATED VOLTAGE

For RSC, the stator current reference can be generated based on instantaneous power theory and is expressed as

$$\begin{cases} i_{sdref} = 0.667(u_{sd}P_{sref} + u_{sq}Q_{sref})/U_s^2 \\ i_{sqref} = 0.667(u_{sq}P_{sref} + u_{sd}Q_{sref})/U_s^2 \end{cases} \tag{15}$$

where U_s is the stator voltage amplitude, P_{sref} and Q_{sref} are the active and reactive power references, respectively.

As seen, the stator current reference generation in (15) is irrelevant of generator parameters. The reduced parameter dependency of RSC control is obtained. It is noted that the value in the denominator of (15) exhibits oscillations and would produce non-sinusoidal current reference with higher-order harmonics. However, since PI controllers have limited control bandwidth only in the low-frequency spectrum, they can still be used to regulate the dc components to track their average values regardless of the harmonic ones [18]. Thus, the average active and reactive power can be well tracked.

For the generator, the torque ripples would increase extra mechanical stress on mechanical parts and is preferred to be constant under unbalanced grid voltage conditions. As indicated, the torque contains the oscillating part at twice the grid frequency, which should be controlled to be zero.

Since the ROVI can provide the adequate gain only with the ac signals adjacent to $2\omega_n$ and attenuate the amplitude gains of other frequency signals. Thus, the electromagnetic torque can be directly set as the control input without extracting the oscillating parts. Compared to the conventional approach, the sequence extraction of the positive and negative-sequence voltages and currents are not necessary. Thus, ROVI's input can be obtained by,

$$C_R = T_e = 1.5(\psi_{sd}i_{sq} - \psi_{sq}i_{sd}) \tag{16}$$

Due to the frequency discrimination of the ROVI, it only has the control ability at the resonant frequency and no effect on the dc component. For simplification, the ROVI's reference in the full spectrum is set to zero, i.e., C_{Rref} =0.

Since the active and reactive powers are coupled in the derived d-q axis currents, the ROVI output, regard as the active part, cannot be directly added to the derived d-q model in (6). Thus, a voltage vector is introduced as a multiplier to achieve the corresponding relationship between the d-q axis currents and the active/reactive powers. The modulated rotor voltage $\boldsymbol{U}_{rref}$ is obtained by,

$$\boldsymbol{U}_{rref} = \boldsymbol{E}_{rdq} - \boldsymbol{U}_{PI} - \boldsymbol{U}_{sdq}/U_s^2 \cdot \boldsymbol{U}_{ROVI} \tag{17}$$

where $\boldsymbol{U}_{\mathrm{PI}}$ and $\boldsymbol{U}_{\mathrm{ROVI}}$ are the outputs of the PI and ROVI controllers of RSC, respectively.

As shown, the modulated rotor voltage $\boldsymbol{U}_{rref}$ consists of three parts: the decoupling term $\boldsymbol{E}_{rdq}$ in (8), the PI output $\boldsymbol{U}_{\mathrm{PI}}$ and the ROVI output $\boldsymbol{U}_{\mathrm{ROVI}}$. The PI controller can guarantee to follow the average powers regardless of the network unbalance and frequency deviation. The ROVI will produce twice the grid frequency modulated rotor voltage for the torque ripple reduction. If the grid voltage is ideal and balanced, the electromagnetic torque behaves as constant and then the ROVI output would be null. When the grid voltage is unbalanced, the electromagnetic torque would contain both the dc part and the oscillating part, but the ROVI only generate the twice-grid-frequency signals for torque ripple reduction due to the ability of frequency discrimination. Finally, together with the decoupling term in (8), the modulated rotor voltage for RSC is produced.

For GSC, based on the instantaneous power theory, its commanded current values can be calculated by,

$$\begin{cases} i_{gdref} = 0.667(u_{gd}P_{gref} + u_{gq}Q_{gref})/U_g^2 \\ i_{gqref} = 0.667(u_{gq}P_{gref} + u_{gd}Q_{gref})/U_g^2 \end{cases} \tag{18}$$

Since GSC needs to maintain the constant dc-link voltage, the dc-link voltage control loop is used as the outer control loop to produce the active power reference P_{gref}. Since GSC operate with unity-power-factor, the reactive power reference is set as zero. Thus, (18) can be simplified as,

$$\begin{cases} i_{gdref} = 0.667u_{gd}P_{gref}/U_g^2 \\ i_{gqref} = 0.667u_{gq}P_{gref}/U_g^2 \end{cases} \tag{19}$$

Since the grid voltage is not oriented with the axis, both the d- and q-axis currents contain the active component. As analyzed in [18], the dc-voltage outer control loop has a much lower bandwidth between one-tenth and one-fifth of the inner control loop bandwidth. Its output can be regarded as the dc signal. During network unbalance, although the calculated results in (19) would contain the oscillating components, as analyzed, PI controller can still track the current reference due to the lower control bandwidth.

The total currents injected into the grid consist of DFIG stator currents and GSC currents. For the specific target to reduce torque ripples, the stator negative-sequence currents are fixed under unbalanced grid voltage conditions. However, the GSC negative-sequence currents are flexibly controlled for reinforced behaviors. By flexibly regulating the negative sequence currents of GSC, three available modes can be achieved by as follows: 1) rebalancing total currents; 2) removing twice the grid frequency total active power pulsations; 3) removing twice the grid frequency total reactive power pulsations.

Similar to RSC, the ROVI reference for GSC is set as zero, i.e., C_{Gref} =0. The measured currents and powers are directly used as the control inputs without extracting the oscillating parts. For the available modes, the ROVI control inputs are as follows.

Mode I: For rebalancing total currents, the negative sequence currents are controlled to be zero. The ROVI control input is given by,

$$C_G = \boldsymbol{I}_{tdq} = i_{td} + j \cdot i_{tq} \tag{20}$$

Mode II: For removing the twice grid frequency active power pulsation, the output active power is controlled to be constant. The control input is obtained as,

$$C_G = P_t = 1.5(u_{gd}i_{td} + u_{gq}i_{tq}) \tag{21}$$

Mode III: For removing the twice grid frequency reactive power pulsation, the output reactive power is controlled to be constant. The control input is obtained as,

$$C_G = -jQ_t = -j1.5(u_{gq}i_{td} - u_{gd}i_{tq}) \tag{22}$$

For *Mode I*, the ROVI output is the required *d-q* axis voltage produced by the *d-q* axis current, which is directly added to the *d-q* model in (10). However, when the active or reactive power is used as the control input, the coupling between the powers and the d-q axis currents must be considered. Thus, the grid voltage vector, as a additional multiplier, is employed to obtain the decoupled relationship between the *d-q* axis currents and the powers. The modulated GSC voltage $\boldsymbol{V}_{cref}$ can be obtained by,

$$\boldsymbol{V}_{cref} = \begin{cases} \boldsymbol{E}_{cdq} - \boldsymbol{V}_{\mathrm{PI}} - \boldsymbol{V}_{\mathrm{ROVI}}\,(ModeI) \\ \boldsymbol{E}_{cdq} - \boldsymbol{V}_{\mathrm{PI}} - \boldsymbol{U}_{gdq}/U_g^2 \cdot \boldsymbol{V}_{\mathrm{ROVI}}\,(ModeII, III) \end{cases} \tag{23}$$

where $\boldsymbol{V}_{\mathrm{PI}}$ and $\boldsymbol{V}_{\mathrm{ROVI}}$ are the outputs of the PI and ROVI controllers of GSC, respectively.

The modulated GSC voltage is also made up of three parts: the decoupling term $\boldsymbol{E}_{cdq}$, the PI output $\boldsymbol{V}_{\mathrm{PI}}$ and the ROVI output $\boldsymbol{V}_{\mathrm{ROVI}}$. The PI controller can track the positive sequence currents for average power regulation to maintain the steady-state dc-link voltage. The ROVI would produce the required twice-grid-frequency voltage for the predefined modes, including balanced total currents, constant total active power and constant total reactive power. If the network is ideal and balanced, the control inputs in (20)-(22) are non-oscillatory and the control outputs will be zero, which has no impact on the normal operation of the GSC. During network unbalance, the control inputs contain the oscillating components around twice the grid frequency. Then, the ROVI would produce the required twice the grid frequency modulated GSC voltage to achieve the available modes. Finally, together with the decoupling term in (11), the modulated voltage for GSC is produced.

C. SYSTEM IMPLEMENTATION

Figure 3 presents the block diagram of the proposed coordinated derived current control strategy. It is noted that since RSC and GSC control are separately implemented in two converters, the virtual phase angle for the RSC and the GSC can be different from each other. It means that the virtual phase angles for the RSC and GSC are not necessarily same, which can be independently calculated.

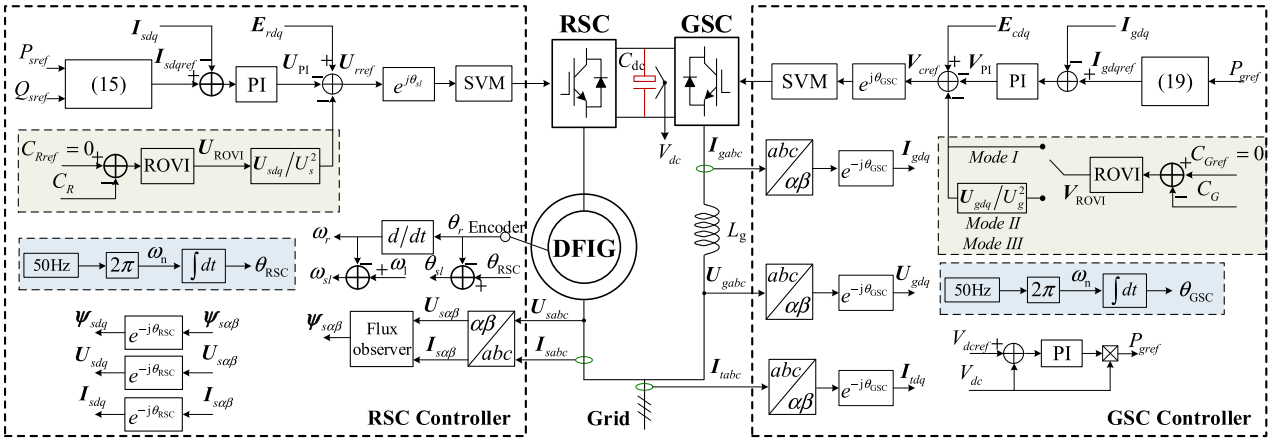

FIGURE 3. Block diagram of proposed control strategy.

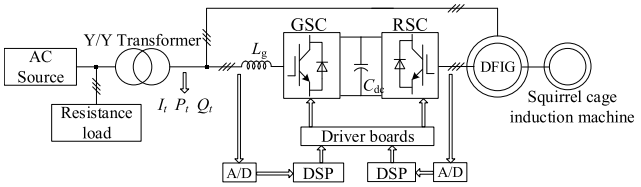

FIGURE 4. Schematic diagram of the laboratory setup.

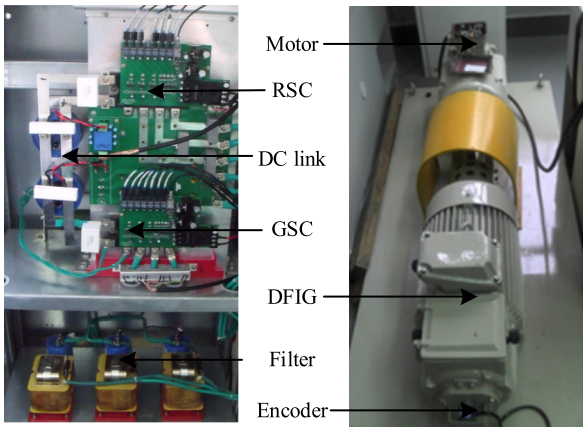

FIGURE 5. Experimental setup of the laboratory setup.

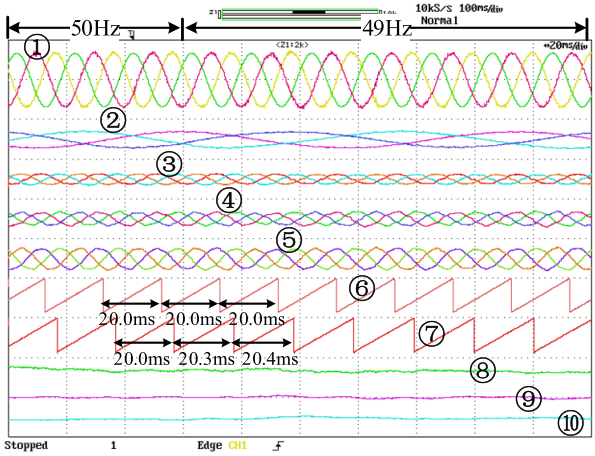

FIGURE 6. Experimental results of the proposed control strategy with frequency deviation. [① stator line-line voltage (300 V/div); ② rotor current (8 A/div); ③ GSC current (20 A/div); ④ total current (30 A/div); ⑤ stator current (30 A/div); ⑥ virtual phase angle; ⑦ voltage phase angle; ⑧ electromagnetic torque (15 Nm/div); ⑨ total active power (1 kW/div); ⑩ total reactive power (1 kVar/div)].

For RSC, the modulated rotor voltage in (17) need be transformed from the virtual phase angle-oriented reference frame to the rotor stationary reference frame, which remains stationary with the rotating rotor at ω_r. Then, based on the rotor angle θ_r acquired by the encoder and the virtual phase angle θ_{RSC} for RSC, the modulated RSC voltage in the rotor stationary reference frame is obtained by,

$$\boldsymbol{U}_m = \boldsymbol{U}_{rref} \cdot e^{j\theta_{sl}} = \boldsymbol{U}_{rref} \cdot e^{j(\theta_{RSC}-\theta_r)} \tag{24}$$

where $\theta_{sl} = \theta_{RSC} - \theta_r$ is the slip angle.

For GSC, the modulated GSC voltage in (23) is required to be transformed into the stationary reference frame. Based on the virtual phase angle θ_{GSC} for GSC, the modulated GSC voltage in the stationary reference frame is written as,

$$\boldsymbol{V}_m = \boldsymbol{V}_{cref} \cdot e^{j\theta_{GSC}} \tag{25}$$

Finally, the space vector modulation is used to generate the switching signals based on the modulated RSC and GSC voltages. The RSC and GSC can operate in the predefined modes with enhanced behaviors. Compared the convention methods, the main advantages of the derived current control strategy can be summarized as follows.

1) All the calculation and implementation in the proposed control strategy are carried out in the virtual phase angle-oriented reference frame. Thus, the need of PLL is completely avoided.
2) The derived stator current control for RSC is used with its references obtained from instantaneous power theory with less parameter dependency.
3) The ROVI with a voltage multiplier is designed to regulate the currents/powers without sequence extraction separations and calculations.

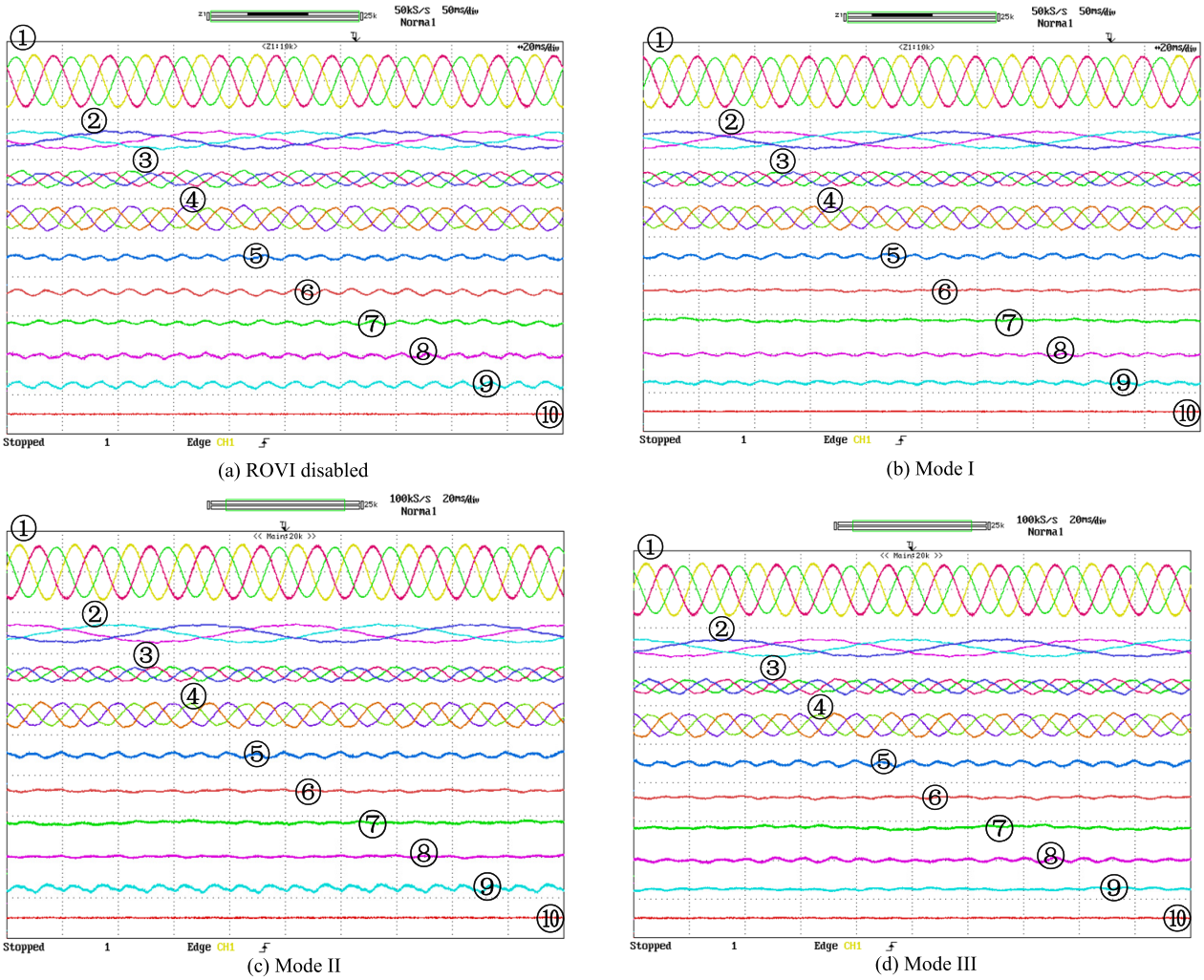

FIGURE 7. Steady performance of the proposed control strategy. [① stator line-line voltage (300 V/div); ② rotor current (8 A/div); ③ GSC current (20 A/div); ④ total current (30 A/div); ⑤ stator current (30 A/div); ⑥ virtual phase angle; ⑦ voltage phase angle; ⑧ electromagnetic torque (15 Nm/div); ⑨ total active power (1 kW/div); ⑩ total reactive power (1 kVar/div)].

IV. EXPREMENTAL RESULTS

The experimental tests on a 1kW-scaled laboratory setup are carried out to validate the effectiveness of the proposed control strategy. The parameters and configurations are given in Table 1 and Figure 4, respectively.

In the laboratory setup, DFIG is driven by a squirrel-cage induction motor and the unbalanced grid is simulated by a Chroma programmable ac source 61704. Since Chroma is a unidirectional ac source, a local resistive load is added. The switching frequency of RSC and GSC is 10 kHz. Since the large inertia of the wind turbine results in large mechanical time constant, the rotor speed is initially set at 800 r/min with its synchronous speed being 1000 r/min.

Figure 6 gives the experimental results of the proposed control strategy with 1.0 Hz frequency deviation. In the following tests, since the inertia response of the DFIG is not studied in this paper, the stator active and reactive power references are simply set as fixed values at 1000 W and 0 Var, respectively. In practice, since there are the switching loss, the magnetizing loss and the copper loss, the total output active power decreases to 650W. The total harmonic distortions (THD) of stator and rotor currents are around 2.9% and 2.2%, respectively. This is mainly caused by the tooth harmonics of the generators. It is seen that the generator can remain satisfactory performance with steady power and electromagnetic torque even if there is frequency changing. In other words, the derived current control is robust to frequency deviations allowed in grid codes [22], [23]. As a result, the frequency adaptability of the proposed control strategy is confirmed.

Figure 7 gives the steady performance of the proposed control strategy. In the tests, the grid frequency is set at 50.0 Hz and the voltage unbalance factor (VUF) is set at 5.6%. Since the dc capacitor in this setup is enough large with the adequate buffer, the dc voltage fluctuations are not so apparent in the following tests. For clear statements, current unbalance factor (CUF) is introduced to represent the radio of the amplitude of the negative-sequence current to that

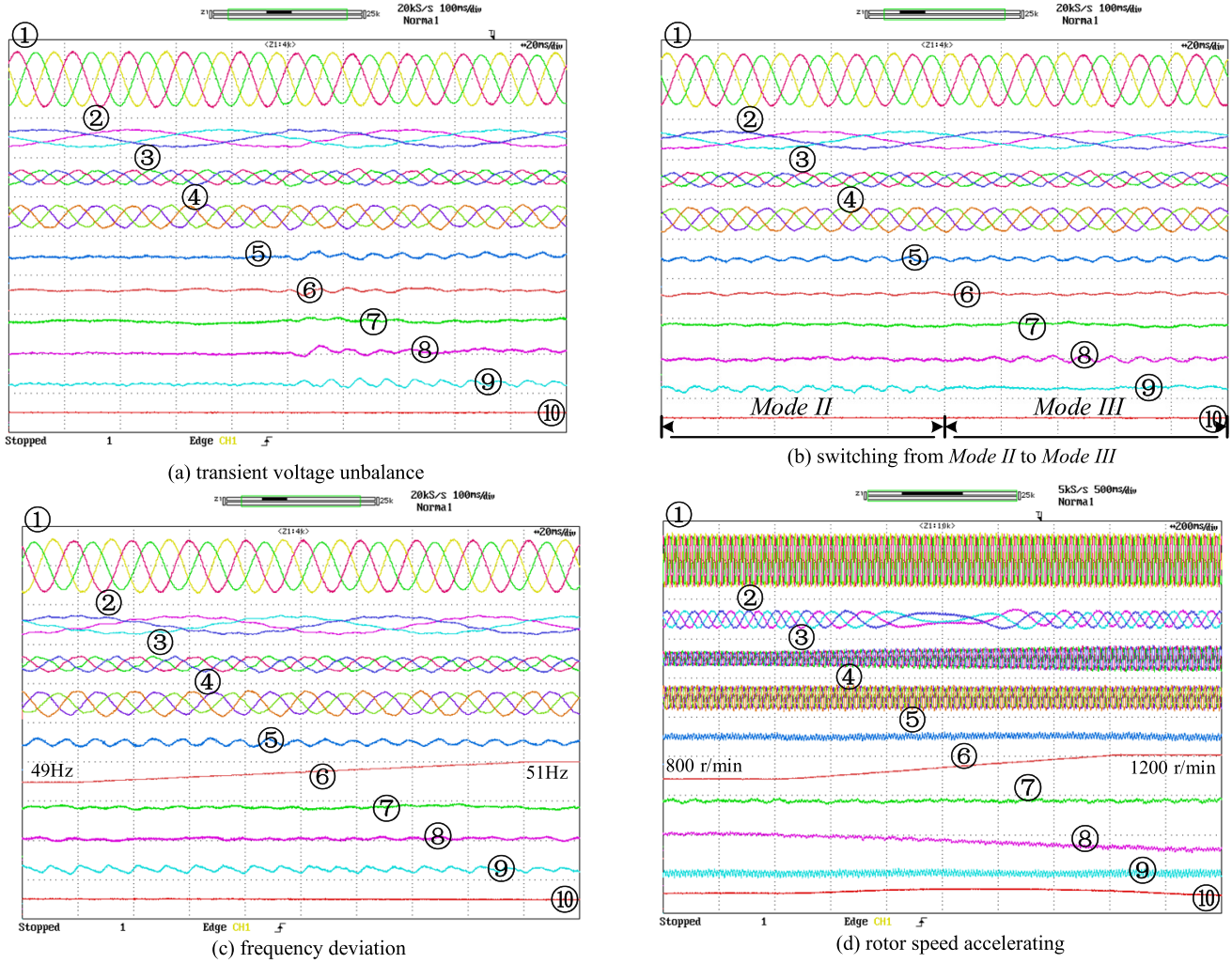

(a) transient voltage unbalance

(b) switching from *Mode II* to *Mode III*

(c) frequency deviation

(d) rotor speed accelerating

FIGURE 8. **Dynamic responses of the proposed control strategy. [① stator line-line voltage (300 V/div); ② rotor current (8 A/div); ③ GSC current (20 A/div); ④ total current (30 A/div); ⑤ stator current (30 A/div); ⑥ virtual phase angle; ⑦ voltage phase angle; ⑧ electromagnetic torque (15 Nm/div); ⑨ total active power (1 kW/div); ⑩ total reactive power (1 kVar/div)].**

of the positive-sequence current. In Figure 7(a), since the unbalanced control is inactive with ROVIs disabled, the stator currents are greatly unbalanced with its CUF being 12.5%. The oscillating amplitude of the torque is around 8.5%. For the overall grid-connected performance, the total current is highly unbalanced and its CUF is around 21.3%. Then, together with unbalanced voltages, the oscillating amplitudes of the total active and reactive power are approximately 6.4% and 8.7%, respectively. In Figure 7(b)-(d) with ROVIs enabled, the amplitude of torque ripples is greatly decreased from 8.5% to 1.1%. For GSC, when *Mode I* is active in Figure 7(b), the CUF of the total currents is decreased from 21.3% to 2.1% and then the active and reactive power pulsations are partly suppressed. In Figure 7(c), since *Mode II* is available, the oscillating amplitude of the total active power obviously decreases to nearly 1.1%. Then, when switched to *Mode III* in Figure 7(d), the total reactive power pulsations are nearly 1.0%. Therefore, the coordinated derived control strategy can accomplish the predefined modes and then enhance the overall performance of DFIG system.

Table 2 summarizes the CUF of the total current, the oscillating amplitude of total power and the oscillating amplitude of electromagnetic torque with *Mode I/II/III* under unbalanced grid voltage conditions. It is confirmed that the coordinated derived control strategy can greatly reinforce the grid-connected behaviors on the reduction of the torque ripples, the rebalance of total current and the mitigation of oscillating powers under unbalanced grid voltage conditions.

Figure 8 gives the dynamic responses of the proposed control strategy. In Figure 8(a)-(d), RSC reduces the torque ripples and GSC is to remove the oscillating parts of total active power with *Mode II* active. In Figure 8(a), during a transient voltage unbalance (VUF=5.6%), the oscillating parts of electromagnetic torque and total active power are rapidly eliminated around 40 ms. Figure 8(b) presents the dynamic responses with *Mode II* switching to *Mode III*.

TABLE 2. Comparisons with different modes.

	ROVI disabled	*Mode*		
		I	*II*	*III*
I_r *CUF* (%)	21.3%	2.2%	4.9%	8.9%
P_t oscillating amplitude (%)	6.4%	3.9%	1.1%	6.3%
Q_t oscillating amplitude (%)	8.7%	4.8%	7.1%	1.0%
T_e oscillating amplitude (%)	8.5%	1.1%		

As seen, the switching process is smooth without overshoot current and oscillating power. In Figure 8(c), the frequency changing from 49.0Hz to 51.0 Hz is set. The overall performance of DFIG system remain steady with no obvious difference from Figure 7(c). The robustness of the proposed control strategy against frequency deviations is confirmed. In Figure 8(d), the rotor speed accelerates from 800 r/min (sub-synchronous) to 1200 r/min (super-synchronous). It is seen that the total active power remains steady with a smooth increase during the rotor speed accelerating.

Consequently, it is validated that the coordinated derived current control can provide reinforced performance and frequency adaptability with unbalanced voltages and frequency deviations.

V. CONCLUSION

This paper presents a coordinated derived current control strategy of RSC and GSC. It synchronizes to the grid through virtual phase angle produced by nominal frequency and then implements in an arbitrary reference frame without PLL. The derived d-q axis currents are used as feedback currents from the DFIG stator and GSC currents with virtual-angle-based Park Transformations. Compared to the conventional rotor current control, the derived current control results in less dependency of the generator parameters. However, due to the absence of PLL, the active/reactive components and the d-q axes components are coupling. To address this, ROVI multiplied by a voltage vector is designed as the resonant controller to directly regulate the measured powers/currents containing both the dc part and the oscillating part without sequence extractions. Finally, the experimental results of the proposed control strategy are presented. It is confirmed that the proposed coordinated derived current control strategy can guarantee the satisfactory performance and frequency adaptability under unbalanced grid voltage conditions.

REFERENCES

[1] *Global Energy Transformation: A Roadmap to 2050*, IRENA, Masdar City, United Arab Emirates, 2019.
[2] F. Blaabjerg and K. Ma, "Wind energy systems," *Proc. IEEE*, vol. 105, no. 11, pp. 2116–2131, Nov. 2017.
[3] Y. Chen, M. Chen, Z. Tian, and Y. Liu, "Voltage unbalance management for high-speed railway considering the impact of large-scale DFIG-based wind farm," *IEEE Trans. Power Del.*, early access, Oct. 25, 2019, doi: 10.1109/TPWRD.2019.2949563.
[4] Q. Guo, S. Xin, H. Sun, Z. Li, and B. Zhang, "Rapid-charging navigation of electric vehicles based on real-time power systems and traffic data," *IEEE Trans. Smart Grid*, vol. 5, no. 4, pp. 1969–1979, Jul. 2014.
[5] *Technical Rule for Connecting Wind Farm to Power System*, Standard GB/T 19963, 2011.
[6] *Establishing a network Code on Requirements for Grid Connection of Generators*, document Commission Regulation (EU) 2016/631, 2016.
[7] M. A. Shuvra and B. Chowdhury, "Distributed dynamic grid support using smart PV inverters during unbalanced grid faults," *IET Renew. Power Gener.*, vol. 13, no. 4, pp. 598–608, Mar. 2019.
[8] T. Wang, L. Kong, H. Nian, and Z. Q. Zhu, "Coordinated elimination strategy of low order output current distortion for LC-filtered DFIG system based on hybrid virtual impedance method," *IEEE Trans. Power Electron.*, vol. 34, no. 8, pp. 7502–7520, Aug. 2019.
[9] D. Sun and X. Wang, "Low-complexity model predictive direct power control for DFIG under both balanced and unbalanced grid conditions," *IEEE Trans. Ind. Electron.*, vol. 63, no. 8, pp. 5186–5196, Aug. 2016.
[10] H. Nian, C. Wu, and P. Cheng, "Direct resonant control strategy for torque ripple mitigation of DFIG connected to DC link through diode rectifier on stator," *IEEE Trans. Power Electron.*, vol. 32, no. 9, pp. 6936–6945, Sep. 2017.
[11] H. Nian, Z. Zhu, and P. Cheng, "Direct power control of doubly fed induction generator without phase-locked loop in synchronous reference frame during frequency variations," *IET Renew. Power Gener.*, vol. 9, no. 6, pp. 576–586, Aug. 2015.
[12] Y. Xu and Y. Cao, "Sub-synchronous oscillation in PMSGs based wind farms caused by amplification effect of GSC controller and PLL to harmonics," *IET Renew. Power Gener.*, vol. 12, no. 7, pp. 844–850, May 2018.
[13] J. Liu, W. Yao, J. Wen, J. Fang, L. Jiang, H. He, and S. Cheng, "Impact of power grid strength and PLL parameters on stability of grid-connected DFIG wind farm," *IEEE Trans. Sustain. Energy*, vol. 11, no. 1, pp. 545–557, Jan. 2020.
[14] D. Zhu, S. Zhou, X. Zou, and Y. Kang, "Improved design of PLL controller for LCL-type grid-connected converter in weak grid," *IEEE Trans. Power Electron.*, vol. 35, no. 5, pp. 4715–4727, May 2020, doi: 10.1109/TPEL.2019.2943634.
[15] D. Yang, X. Wang, F. Liu, K. Xin, Y. Liu, and F. Blaabjerg, "Symmetrical PLL for SISO impedance modeling and enhanced stability in weak grids," *IEEE Trans. Power Electron.*, vol. 35, no. 2, pp. 1473–1483, Feb. 2020.
[16] Y. Gui, M. Li, J. Lu, S. Golestan, J. M. Guerrero, and J. C. Vasquez, "A voltage modulated DPC approach for three-phase PWM rectifier," *IEEE Trans. Ind. Electron.*, vol. 65, no. 10, pp. 7612–7619, Oct. 2018.
[17] Y. Gui, X. Wang, H. Wu, and F. Blaabjerg, "Voltage modulated direct power control for a weak grid-connected voltage source inverter," *IEEE Trans. Power Electron.*, vol. 34, no. 11, pp. 11383–11395, Nov. 2019.
[18] H. Nian, P. Cheng, and Z. Q. Zhu, "Coordinated direct power control of DFIG system without phase-locked loop under unbalanced grid voltage conditions," *IEEE Trans. Power Electron.*, vol. 31, no. 4, pp. 2905–2918, Apr. 2016.
[19] Y. Gui, X. Wang, and F. Blaabjerg, "Vector current control derived from direct power control for grid-connected inverters," *IEEE Trans. Power Electron.*, vol. 34, no. 9, pp. 9224–9235, Sep. 2019.
[20] P. Cheng, H. Nian, C. Wu, and Z. Q. Zhu, "Direct stator current vector control strategy of DFIG without phase-locked loop during network unbalance," *IEEE Trans. Power Electron.*, vol. 32, no. 1, pp. 284–297, Jan. 2017.
[21] P. Cheng, J. Tang, S. Wang, Q. Li, and C. Wu, "Control scheme of DFIG's RSC and GSC with self-synchronization approach," in *Proc. Int. Conf. Power Syst. Technol. (POWERCON)*, Guangzhou, China, Nov. 2018, pp. 1339–1344.
[22] *Power Quality-Frequency Deviation for Power System*, document GB/T 15945, 2008.
[23] *Compatibility Levels for Low-Frequency Conducted Disturbances and Signaling in Public Low-Voltage Power Supply System*, document IEC 61000-2-2, 2002.

PENG CHENG was born in Liaoning, China. He received the B.S. and Ph.D. degrees in electrical engineering from Zhejiang University, Hangzhou, China, in 2011 and 2016, respectively.

He is currently an Assistant Professor with the Department of China Institute of Energy and Transport Integration Development, North China Electric Power University, China. His current research interests include multiconverter power systems and renewable power generation, particularly wind power generation.

CHAO WU (Member, IEEE) was born in Hubei, China. He received the B.Eng. degree from the Hefei University of Technology, Hefei, China, in 2014, and the Ph.D. degree from Zhejiang University, Hangzhou, China, in 2019, all in electrical engineering.

He is currently a Postdoctoral Researcher with the Department of Energy Technology, Aalborg University, Aalborg, Denmark. His current research interests include cooperative control of multiconverter systems, particularly the control and operation of doubly fed induction generators for dc connection.

JING MA (Senior Member, IEEE) was born in Hebei, China, in February 1981. He received the B.S. and Ph.D. degrees from North China Electric Power University, China, in 2003 and 2008, respectively.

He was a Visiting Research Scholar with the Bradley Department of Electrical and Computer Engineering, Virginia Polytechnic Institute and State University, from 2008 to 2009. He is currently a Full Professor with the School of Electrical and Electronic Engineering, North China Electric Power University, China. His major interests include power system equipment modeling, diagnoses, and protection.

FREDE BLAABJERG (Fellow, IEEE) received the Ph.D. degree in electrical engineering from Aalborg University, in 1995.

He was with ABB-Scandia, Randers, Denmark, from 1987 to 1988. He became an Assistant Professor, in 1992, an Associate Professor, in 1996, and a Full Professor of power electronics and drives, in 1998. In 2017, he became a Villum Investigator. He is honoris causa at University Politehnica Timisoara (UPT), Romania, and Tallinn Technical University (TTU), Estonia. His current research interests include power electronics and its applications, such as in wind turbines, PV systems, reliability, harmonics, and adjustable speed drives. He has published more than 600 journal articles in the fields of power electronics and its applications. He is the coauthor of four monographs and editor of ten books in power electronics and its applications.

Dr. Blaabjerg received 32 IEEE Prize Paper Awards, the IEEE PELS Distinguished Service Award, in 2009, the EPE-PEMC Council Award, in 2010, the IEEE William E. Newell Power Electronics Award, in 2014, the Villum Kann Rasmussen Research Award, in 2014, the Global Energy Prize, in 2019, and the 2020 IEEE Edison Medal. He was the Editor-in-Chief of the IEEE TRANSACTIONS ON POWER ELECTRONICS, from 2006 to 2012. He is nominated in 2014–2019 by Thomson Reuters to be between the most 250 cited researchers in engineering in the world. He has been a Distinguished Lecturer of the IEEE Power Electronics Society, from 2005 to 2007, and the IEEE Industry Applications Society, from 2010 to 2011 and from 2017 to 2018. He is also serving as the President of the IEEE Power Electronics Society, for the period of 2019–2020. He is also the Vice-President of the Danish Academy of Technical Sciences.